Fig. 1.   Lys to Arg substitution mutations conferring A3G resistance to HIV-1 Vif-dependent degradation. (A) WT A3G and mutants. Numbers 1 to 14, shown above the diagram, refer to the 14 Lys residues illustrated in Fig. S2 [i.e., at positions 63, 76, 79, 99, 113, 141, 180, 249, 270, 297, 301, 303, 334, and 344 (K1–14), respectively (position numbers indicated below the figure)]. Five mutants have Arg substitutions in K1–9, 1–4, 5–9, 8–14, and 10–14 and were designated as K (1–9)R, K(1–4)R, K (5–9)R, K(8–14)R, and K(10–14)R, respectively. (B) and (C) Vif-dependent degradation of A3G mutants. 293T cells were transfected with or without pcDNA-HVif plus the indicated A3G expression plasmid. The amounts of cellular A3G from cells transfected with or without the Vif-expressing plasmid were compared by Western blot analysis using anti-A3G antibody. In (B), D128K, a defective A3G that does not bind Vif, was used as a positive control. (D) Effect of increasing levels of Vif expression on degradation of WT A3G and A3G mutant K(10, 11, 12, 13)R. Two micrograms of each A3G expression plasmid was used. For Vif expression, pcDNA-HVif/pcDNA 3.1 (-) plasmids (8 μg) were used at the following ratios: 8:0 (lanes 1, 8, 15); 1:1 (lanes 2 and 9); 3:5 (lanes 3 and 10); 1:3 (lanes 4 and 11); 1:15 (lanes 5 and 12); 1:79 (lanes 6 and 13); and 0:8 (lanes 7 and 14). Anti-β-tubulin antibody was used as a control.

The information available thus far concerning the interaction between Vif and A3G in the Ub ligase complex suggests that there may be a specific mechanism for Ub conjugation of the A3G protein. Yet, despite our knowledge that the participants interact with each other in the EloB/C-Cul5-Vif-A3G complex, the details of how the complex dictates A3G polyubiquitination and subsequent degradation remain unclear. In part, this is due to the lack of complete structural information about the A3G and Vif proteins and the complex they form. Our approach to this problem was to construct a structural model of hA3G for testing which Lys residues may serve as targets for ubiquitination. Based on the structural model we selected 14 surface-exposed Lys and established that only four of these residues (Lys-297, 301, 303, and 334) in the C-terminal domain (CTD) are essential for Vif-induced degradation of A3G. In addition, we demonstrated that a "super" A3G (S-A3G) with all of these four residues mutated to Arg was resistant to degradation by Vif and was able to block replication of WT HIV-1. Taken together, our results provide insights into the determinants governing Vif-mediated A3G inactivation and should stimulate and aid efforts to develop antiviral strategies that focus on disruption of the Vif-A3G interaction.

Results

The A3G Model Shows 14 Lys Residues with Substantially Exposed ε-Amino Groups.
The goal of the present study was to identify Lys residues in hA3G that become ubiquitinated in a Vif-dependent manner, resulting in subsequent degradation by the proteasome pathway. In general, during polyubiquitination, the first ubiquitin is typically conjugated to an ε-amino group of an exposed Lys within the target protein (16). For hA3G, the amino acid sequence contains 20 Lys residues (Fig. S1), 14 of which are completely accessible on the surface in a model structure (Fig. S2). Our model structure was based on the X-ray structures of the A3G catalytic domain (32) and the related homodimeric A2 protein (33) and was generated to guide our selection of the most solvent accessible Lys residues. Homology models for the NTD

and CTD were generated using the program Modeller (http:// salilab.org/modeller) (34) and the relative positioning of the domains in the A3G model was based on the arrangement of the monomeric A2 proteins in the homodimer. The most exposed Lys residues were found at positions 63, 76, 79, 99, 113, 141, 180, 249, 270, 297, 301, 303, 334, and 344, and are highlighted in blue in the amino acid sequence of hA3G (Fig. S1). In the following discussion they are designated as K1–14, respectively.

Arg Substitutions for Lys-297, 301, 303, and 334 Render A3G Resistant to Vif-Mediated Degradation.
In an effort to identify which Lys residue(s) may be responsible for A3G ubiquitination, Arg substitutions were made at the selected 14 positions in A3G and mutants were assayed for intracellular degradation. In particular, we tested whether HIV-1 Vif enhanced degradation ("Vif sensitivity") of A3G was affected. Initially, 14 point mutants were constructed and each mutant remained Vif-sensitive (Fig. S3). This suggested that most likely, more than one residue might be required for conversion to a Vif-resistant phenotype.

To address this question (i.e., whether several Lys residues may be involved), a series of mutants was constructed, each containing changes for a number of Lys residues (Fig. 1). Five mutants, K (1–9)R, K(1–4)R, K (5–9)R, K(8–14)R, and K(10–14)R, with Arg substitutions at positions K1–9, 1–4, 5–9, 8–14, and 10–14, respectively, were generated (Fig. 1A) and the presence of A3G was probed by Western blot analysis (see legend to Fig. 1). As expected, WT A3G was not detectable when co-expressed with HIV-1 Vif (Vif-sensitive), while the level of the D128K A3G mutant protein that lacks the ability to bind HIV-1 Vif (27–30) was unchanged in the presence of Vif (Vif-resistant) (Fig. 1B). The K (1–9)R, K(1–4)R, and K(5–9)R mutants were sensitive to Vif, i.e., they behaved like WT A3G in this assay. In contrast, protein levels of the K(8–14)R and K(10–14)R mutants were unaffected (i.e., Vif-resistant) (Fig. 1B). This suggested that all five Lys residues from 10 through 14, or a subset thereof, were critical for mediation of Vif-dependent ubiquitination.
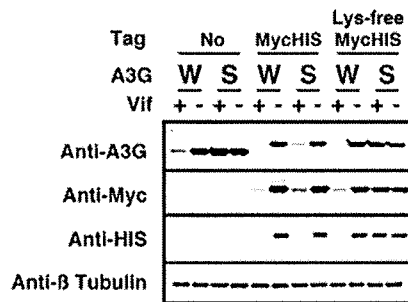
Tag	No		MycHIS		Lys-free MycHIS	
A3G	W	S	W	S	W	S
Vif	+	-	+	-	+	-	+	-
Anti-A3G						
Anti-Myc						
Anti-HIS						
Anti-β Tubulin						

Fig. 2. Effect of a MycHIS tag at the C-terminal end of A3G. WT A3G (W) or S-A3G (S) without a tag (No), with a MycHIS tag or the Lys-free MycHIS tag were expressed in the presence or absence of Vif in 293T cells. A3G was detected by Western blot with anti-A3G antibody (Anti-A3G), anti-Myc tag monoclonal antibody (Anti-Myc), or anti-(His₆) tag antibody (Anti-HIS).

To resolve this point, a second series of A3G mutants with different permutations of the four substitutions in residues 10–14 was evaluated. Only K(10, 11, 12, 13)R was completely Vif-resistant, although K(10, 12, 13, 14)R and K(10, 11, 13, 14)R were partially resistant (Fig. 1*C*). This result demonstrated that Lys residues 10, 11, 12, and 13 are critical determinants of HIV-1 Vif-dependent ubiquitination of A3G, since Arg substitutions in these residues abolished Vif sensitivity, Furthermore, three substitutions within the four residues conferred varying degrees of A3G sensitivity to Vif. To corroborate these conclusions, we compared the amounts of A3G WT and K(10–13)R proteins for varying ratios of pcDNA-HVif/pcDNA 3.1 (-). While significant WT A3G protein was present at low Vif concentrations (Fig. 1*D*, lanes 4–6), no difference in protein amounts was observed for the K(10–13)R mutant at every concentration of Vif that was tested (Fig. 1*D*, lanes 8–13). Thus, K(10–13)R is resistant to Vif-mediated degradation and we will refer to mutant K(10–13)R as "super" A3G (S-A3G) below. We also observed S-A3G Vif resistance in nonpermissive SupT1 T-cell lymphocytes (Fig. S4).

The Additional C-Terminal Tag of A3G Can Mediate Ubiquitination-Induced Proteasomal Degradation. In an initial phase of this study, quite unexpectedly, we found that an A3G mutant with all 14 Lys residues changed to Arg and also having a C-terminal tag was sensitive to Vif-dependent degradation. This surprising result prompted us to test whether the two Lys residues in the C-terminal A3G tag (MycHIS) might become ubiquitinated. We therefore constructed A3G expression plasmids with a Lys-free MycHIS tag and compared the Vif sensitivity of this construct with that of untagged and conventional MycHIS tagged WT and S-A3G plasmids. As clearly seen in Fig. 2, S-A3G protein levels were similar in the absence or presence of HIV-1 Vif. In contrast, the addition of the C-terminal MycHIS tag rendered S-A3G (S) susceptible to the presence of Vif, exhibiting behavior very similar to that of WT A3G. This was reversed when the Lys-free MycHIS version of S-A3G was used. In this case, complete resistance to Vif-dependent A3G degradation was noted. These findings demonstrated that the two Lys in the C-terminal tag can serve as ubiquitination sites. Note that identical protein levels were detected irrespective of the type of antibodies (anti-A3G, anti-Myc or anti-HIS antibodies) used for detection (Fig. 2).

The dependence of A3G polyubiquitination on Vif was investigated by expressing the Lys-free MycHIS tagged A3G in 293T cells. The results showed that no polyubiquitinated S-A3G was detectable, whereas Vif-dependent WT A3G polyubiquitination was clearly observed (Fig. S5). This demonstrates that S-A3G's resistance to Vif-dependent degradation was due to its inability
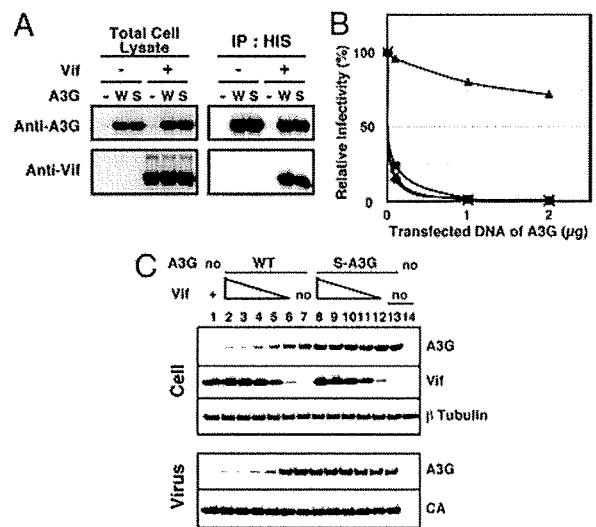

Fig. 3. Effect of incorporation of the K(10, 11, 12, 13)R mutant (S-A3G) into WT or *vif*-deficient virions on infectivity in a single-cycle replication assay. (*A*) 293T cells were cotransfected with pcDNA-HVif and either empty (-), WT (W), or S-A3G (S) plasmids having the Lys-free MycHIS tag, using the procedures described in *Materials and Methods*. The MycHIS-tagged proteins were analyzed either directly (*Left*) as "Total Cell Lysate" or following pull-down (binding of the HIS tag to TALON resin) (*Right*) by immunoblotting with the indicated antibodies. (*B*) Virus infectivity; 293T cells were cotransfected with (*i*) pNL4-3 and either WT (▲) or S-A3G (●) expression plasmids or (*ii*) pNL4-3*vif*(-) and either WT (■) or S-A3G (crosses) expression plasmids, using 0, 0.1, 1, or 2 μg of DNA. Where appropriate, the amounts of DNA added for each of the expression plasmids were adjusted with empty vector pcDNA 3.1 (-) to a total of 2 μg. Infectivity values are given relative to the values for 0 μg of the expression plasmids and were set at 100%. (*C*) Analysis of intracellular expression (Cell) and incorporation of WT and S-A3G into virions (Virus) by Western blot. Virions were produced by transfection of pNL4-3 WT/pNL4-3*vif*(-) plus either A3G WT, S-A3G expression plasmid or pcDNA 3.1(-) (shown as "no"). The ratios of pNL4-3 WT to pNL4-3*vif*(-) were as follows. 1:0 (lanes 1, 2 and 8), 1:1 (lanes 3 and 9), 1:3 (lanes 4 and 10), 1:7 (lanes 5 and 11), 1:79 (lanes 6 and 12), and 1:0 (lanes 7 and 13). The intracellular levels of β-tubulin and Vif and the CA level in virions were detected by anti-β-tubulin, anti-Vif, and anti-CA antibodies, respectively.

to be polyubiquitinated, presumably as a consequence of the four Lys mutations.

S-A3G Displays Normal Vif Binding. Abrogation of Vif binding by A3G could also confer resistance to Vif-dependent degradation, as was observed for the D128K mutant (27–30). It therefore seemed prudent to determine whether Arg substitutions at A3G residues 297, 301, 303, and 334 would in any way interfere with A3G's ability to bind Vif. We expressed WT and S-A3G (bearing the Lys-free MycHIS tag) in the presence of the proteasome inhibitor MG132 (2 μM), with or without Vif. Intracellular A3G-Vif complexes were pulled down with Talon beads via the HIS portion of A3G's C-terminal tag and the complexes were detected by either anti-A3G or anti-Vif antibodies (Fig. 3*A*). Coprecipitated complexes of WT or S-A3G contained very similar amounts of Vif, indicating that no impairment of Vif binding resulted from the mutations in S-A3G. As expected, no Vif was detected in the controls.

S-A3G Inhibits HIV-1 Infection. To assess the implications of S-A3G's resistance toward Vif-dependent proteasomal degradation, we tested whether S-A3G exhibited any antiviral activity against HIV-1. To this end, we compared the infectivity of WT and *vif*-deficient HIV-1 in the presence of WT or S-A3G in a single-round replication assay. Since A3G expression levels and the extent of the antiviral effect vary for different virus-producer

cell lines (35, 36), we measured infectivity in this assay as a function of the amount of transfected DNA. Comparing infectivity for a given amount of A3G to infectivity in the absence of A3G was termed "relative infectivity." Interestingly, using 0.1 and 2.0 μg WT A3G DNA for transfection reduced the infectivity of *vif*-deficient HIV-1 to 24 and 0.8%, respectively, while only marginally affecting the infectivity of WT HIV-1 (95 and 71% with 0.1 and 2.0 μg, respectively) (Fig. 3*B*). In contrast, S-A3G suppressed the infectivity of *vif*-deficient as well as WT HIV-1 significantly, consistent with its Vif-resistant phenotype. Furthermore, we could show that a deaminase-deficient version (E259Q) of S-A3G had less antiviral activity than S-A3G against WT and *vif*-deficient HIV-1 (Fig. S6). Note, too, that in the absence of Vif, E259Q mutants derived from WT and S-A3G had the same levels of inhibitory activity (Fig. S6*B*). Collectively these results suggest that the catalytic activity and the antiviral function of S-A3G and WT A3G are equivalent.

To determine whether the inhibitory effect of S-A3G on WT HIV-1 infectivity is correlated with a defect in efficient incorporation of S-A3G into virus particles, we analyzed the amounts of intracellular A3G and A3G packaged into virions as a function of Vif expression (i.e., by transfecting different ratios of pNL4–3/pNL4–3 *vif*(-) together with either WT A3G or S-A3G) (Fig. 3*C*). As Vif expression was increased, the steady state levels of intracellular WT A3G were decreased (Cell, lanes 2–6), while the levels of S-A3G protein were not affected (Cell, lanes 8–12). Concomitant with the decrease in protein levels of intracellular WT A3G, its incorporation into virions was also reduced (Virus, lanes 2–6), while under identical experimental conditions, S-A3G packaging was not significantly affected (Virus, lanes 8–12). These findings demonstrate that S-A3G incorporation into HIV-1 virions is independent of Vif. Therefore, efficient packaging of S-A3G into HIV-1 virus particles occurs and allows S-A3G to exert its inhibitory effect on viral infectivity.

The Critical Residues Involved in Vif-Mediated A3G Degradation Cluster at the C Terminus of the Protein. Identification of the Lys residues crucial for Vif-mediated A3G degradation in conjunction with the molecular model for the protein allowed us to determine their location. All 14 candidate Lys are displayed on the model in Fig. 4. As can be readily observed, the critical residues involved in ubiquitination and proteasomal degradation of A3G (i.e., Lys 297, 301, 303, and 334) cluster in one region of the molecule. This area is located at the opposite end of the known interaction region with Vif (D128, P129, and D130) (31). Interestingly, the critical Lys residues are also close to the C terminus of the polypeptide chain, with K334 located within approximately 13Å. Note that this model also positions the Lys residues of the MycHIS tag in the same general area (Fig. 4*A*, green), possibly explaining our findings regarding Vif-sensitivity of MycHIS tagged S-A3G.

Discussion

The goal of the present study was to provide information about HIV-1 Vif-induced degradation of hA3G, in particular the initial polyubiquitination step (i.e., conjugation of Ub to Lys residues in A3G). Using structure-based mutagenesis as our experimental approach, we identified four Lys residues at positions 297, 301, 303, and 334 in the CTD of A3G that are critical for Vif-dependent degradation. Mutation of these residues to Arg generated a protein, S-A3G, which is resistant to intracellular degradation mediated by HIV-1 Vif. Importantly, the interaction between WT A3G and S-A3G with Vif is very similar and S-A3G is incorporated into WT and *vif*-deficient viral particles to the same extent. In addition, S-A3G dramatically reduces the infectivity of both WT and *vif*-deficient HIV-1 (Fig. 3).

To evaluate ubiquitination of A3G at the structural level, we constructed a model of full-length A3G (Fig. S2) based on the
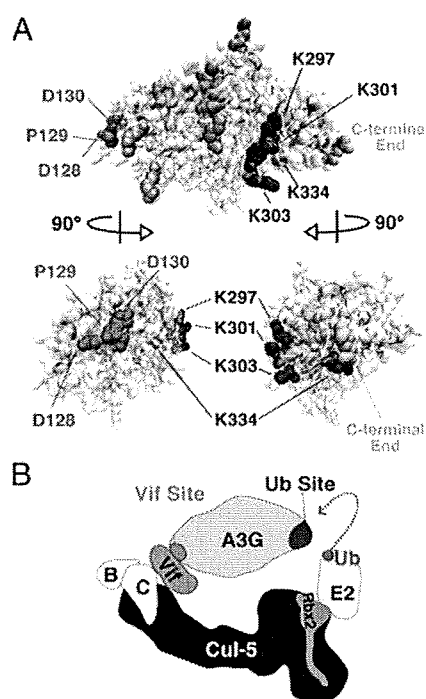

Fig. 4. Region of A3G involved in ubiquitination around Lys residues 297, 301, 303, and 334 and Vif binding mapped onto the structural model. (*A*) Side and 90°-rotated (counterclockwise or clockwise) views of the model in surface representation. Lys residues 297, 301, 303, and 334 are shown in blue, all of the other Lys in cyan, the C-terminal end of A3G in green, and residues D128, P129, and D130 responsible for Vif-binding in red. (*B*) Cartoon illustration of the A3G/Vif/ElonginB/C/Cul-5/Rbx2/E2 complex. The ubiquitination sites on the A3G substrate are marked in blue and the Vif binding site in orange.

crystal structures of the A3G catalytic domain (32) and A2 (33), yielding a domain arrangement of N- and C-terminal domains similar to the individual subunits in homodimeric A2. The structures of the individual domains are very similar to those of other cytidine deaminases and are characterized by a five-stranded mixed beta sheet and five alpha helices. The current CTD of our model is not substantially different from the CTD structures that were recently determined by X-ray crystallography and NMR (32, 37–39). Since we created and used our homology model to guide the current mutagenesis, several other models of A3G have become available (40, 41). Most exhibit a domain disposition similar to the one shown here. Very recently a divergent model has been proposed in which the domains are rotated and the ß-sheet arrangement seen in A2 is not retained (39). Although in this model the details in location of Lys residues will vary, the fact that the Vif interaction site and the critical C-terminal Lys cluster are found at opposite ends of the molecule is still valid.

Even though mutation of these four Lys to Arg residues is the minimum requirement for blocking ubiquitination of A3G, it is of interest to evaluate whether any of these four residues is more favored than others as targets for modification. Both A3G mutants K(10, -, 12, 13, 14)R and K(10, 11, -, 13, 14)R are only partially resistant to ubiquitination compared with A3G K(10, 11, 12, 13, -)R, the molecule termed S-A3G (Fig. 1*C*). This suggests that Lys-301 and Lys-303 (K11 and K12, respectively) are used to a lesser extent than Lys-297 and Lys-334 (K10 and K13, respectively) for ubiquitination. Indeed, it is entirely possible that Lys-297 and Lys-334 represent the two required Lys for Vif-induced A3G degradation and that the two Lys that follow Lys 297, Lys 301 one turn further down the helix and Lys-303 in the following helix, may be able to partially substitute as targets

(Fig. S1). Interestingly, Lys-297 and 334, the most sensitive of the four residues, are highly conserved among primate A3Gs compared with Lys-301 and 303 (Fig. S7).

Surprisingly, in a mutagenesis study similar to the work reported here, Dang et al. found that mutation of all 20 Lys residues in A3G to Arg had no effect on Vif-induced degradation of A3G (42). In an additional test of our model, we also mutated all 20 Lys in A3G (A3G 20K/R) and assayed Vif sensitivity, as well as antiviral activity. Our data showed that like K(1–14)R (the mutant in which all surface-exposed Lys were changed to Arg), A3G 20K/R, 19K/R, and 17K/R were also resistant to Vif-dependent degradation (Fig. S8A). Moreover, the results indicated that A3G 20K/R, like S-A3G, can suppress virus infectivity even in the presence of Vif (Fig. S8B). These findings differ from the report by Dang et al. (42), but the reasons for the apparent discrepancy between our results and those published previously are not clear.

In contrast to the residues that are involved in ubiquitination of A3G, amino acids implicated in Vif binding are located in the NTD (43) within the $_{128}$DPD$_{130}$ motif (31, 43) that is embedded in the $_{126}$FWDPDYQ$_{132}$ (25) sequence in a loop preceding helix 4, which protrudes out from the overall structure (Fig. S2). Significantly, this motif resides on a site opposite to the location of residues involved in ubiquitination in the overall structure (Fig. 4A). Consistent with the model, Vif binding by WT A3G and S-A3G are similar, as evidenced by the coimmunoprecipitation results (Fig. 3A).

In the absence of an experimentally determined three-dimensional structure of HIV-1 Vif, predictions about the configuration of the A3G-Vif-ElonginB/C-Cullin-5 E3 Ub ligase complex can only be speculative. Based on the Skp1-Cul1-Rbx1-F box^{Skp2} (SCF) structure (44) we propose the following scenario for positioning A3G in the complex (Fig. 4B). It is generally accepted that the cullins provide a rigid scaffold for positioning donor and acceptor proteins in the ubiquitination reaction catalyzed by E3. Indeed, mutants in Cul 1 that were designed to eliminate the integrity of the scaffold are deficient in Ub catalysis (44). Moreover, studies on the SCF complex suggested that positioning can explain Lys specificity, i.e., which Lys are the targets for ubiquitination. For example, IkB and SnoN, which are among the few ubiquitinated proteins that have been characterized in detail, are ubiquitinated at specific Lys residues by the SCF and SCF-like complexes consistent with their structural positioning (45, 46).

Similarly, our data suggest that Vif-dependent ubiquitination of A3G in the context of a Cul5-based complex specifically occurs on a site that is located at the end of the protein opposite to the region involved in Vif binding. Thus, spatial constraints imposed by the E3 Ub ligase complex involving Cul5 may be an important determinant for Vif-dependent A3G ubiquitination. It is of interest that HIV-2 and SIV$_{mac}$ Vif proteins target the same Lys residues in hA3G as HIV-1 Vif (Fig. S9). Thus, all three Vif proteins might form complexes with similar structural constraints.

Based on the SCF structural data (45, 46), it seems reasonable to assume that the distance between the E2 active-site Cys and the Ub-modification site on the substrate also plays an important role in activity (44, 47). The average distance in the SCF complexes is approximately 60 Å (44, 47). In the present A3G

model, the distance between the $_{128}$DPD$_{130}$ cluster and the critical Lys residues ranges from 45Å to 60Å, very similar to the distance between the E2 active-site Cys and the substrate-binding site within the Cul 5-EloB/C-Vif-Rbx2-E2 complex. Interestingly, in a recent study by Russell et al. on A3F, the Vif binding region was identified as amino acids 283 to 300 (25). Reference to the A3G structural model suggests that the A3F Vif-binding site corresponds to the A3G ubiquitination region where Lys-297, 301, and 303 are located.

In summary, using model-guided mutagenesis, we have identified four Lys residues in the CTD of A3G that are required for Vif-mediated polyubiquitination and degradation. We show that substitution of four critical Lys to Arg (S-A3G) confers Vif-resistance to A3G and restores A3G's antiviral activity irrespective of Vif. At present, since no polymorphisms at these residues have been reported for hA3G, the natural appearance of A3G variants such as S-A3G is highly unlikely. However, identification of a specific target molecule that removes Vif's inhibitory effect on A3G could advance efforts to develop anti-HIV-1 drugs. Similarly, efforts to design specific screening assays for anti-Vif compounds in vitro will benefit from further characterization of the Vif-A3G interplay with respect to proteasomal degradation.

Materials and Methods

Construction of A3G Structure Model. A homology model of A3G was created based on sequence alignment (automated and adjusted by hand) and subsequent use of the program Modeller (http://salilab.org/modeller) (34) with the crystal structure of the A3G catalytic domain (32) (PDB accession code 3E1U) as the template for the individual NTD and CTD domains. The relative positioning of the NTD and CTD of the template was carried out by superimposing the separated domains onto the crystal structure of A2 (33) (PDB accession code 2NYT). The choice of interface between the two halves of A3G was guided by energy considerations of the final models. The current model in which the beta strands form the dimer interface is energetically more favorable than an alternative one with an alpha helical domain interface.

Plasmids and Antibodies. The plasmids and antibodies used in this work are described in the *SI Text*.

Coimmunoprecipitation Assays. To assess Vif-A3G interaction in vivo, a assay was performed. Briefly, 293T cells were cotransfected with an A3G plasmid having a Lys-free MycHIS tag and with pcDNA-HVif. Thirty-six hours post transfection, the cells were incubated for 12 h with 2 μM MG132, a proteasome inhibitor (Sigma). The presence of MG132 makes it possible to detect WT A3G binding to Vif, since the usual proteasomal degradation is blocked. The cells were harvested and then lysed in lysis buffer (150 mM NaCl, 1 mM EDTA, PBS, 1% Triton X-100, 10 μg/mL of RNase A) plus a protease inhibitor mixture (Sigma). TALON beads (Clontech), which bind His, were used to pull down tagged A3G and were washed with lysis buffer. The complex was analyzed by Western blot with anti-A3G rabbit serum or anti-Vif antibody.

Assays for Vif-Dependent Degradation of A3G, Infectivity in LuSIV Cells and Incorporation of A3G Into Virions. These experiments were performed as reported previously (48).

1. Holmes RK, Malim MH, Bishop KN (2007) APOBEC-mediated viral restriction: Not simply editing? *Trends Biochem Sci* 32:118–128.
2. Wedekind JE, Dance GS, Sowden MP, Smith HC (2003) Messenger RNA editing in mammals: New members of the APOBEC family seeking roles in the family business. *Trends Genet* 19:207–216.
3. Sheehy AM, Gaddis NC, Choi JD, Malim MH (2002) Isolation of a human gene that inhibits HIV-1 infection and is suppressed by the viral Vif protein. *Nature* 418:646–650.
4. Conticello SG, Harris RS, Neuberger MS (2003) The Vif protein of HIV triggers degradation of the human antiretroviral DNA deaminase APOBEC3G. *Curr Biol* 13:2009–2013.

5. Marin M, Rose KM, Kozak SL, Kabat D (2003) HIV-1 Vif protein binds the editing enzyme APOBEC3G and induces its degradation. *Nat Med* 9:1398–1403.
6. Mehle A, et al. (2004) Vif overcomes the innate antiviral activity of APOBEC3G by promoting its degradation in the ubiquitin-proteasome pathway. *J Biol Chem* 279:7792–7798.
7. Sheehy AM, Gaddis NC, Malim MH (2003) The antiretroviral enzyme APOBEC3G is degraded by the proteasome in response to HIV-1 Vif. *Nat Med* 9:1404–1407.
8. Stopak K, de Noronha C, Yonemoto W, Greene WC (2003) HIV-1 Vif blocks the antiviral activity of APOBEC3G by impairing both its translation and intracellular stability. *Mol Cell* 12:591–601.

Iwatani et al.

MICROBIOLOGY

9. Yu X, et al. (2003) Induction of APOBEC3G ubiquitination and degradation by an HIV-1 Vif-Cul5-SCF complex. *Science* 302:1056–1060.

10. Henriet S, et al. (2009) Tumultuous relationship between the human immunodeficiency virus type 1 viral infectivity factor (Vif) and the human APOBEC-3G and APOBEC-3F restriction factors. *Microbiol Mol Biol Rev* 73:211–232.

11. Goila-Gaur R, Strebel K (2008) HIV-1 Vif, APOBEC, and intrinsic immunity. *Retrovirology* 5:51.

12. Iwatani Y, et al. (2007) Deaminase-independent inhibition of HIV-1 reverse transcription by APOBEC3G. *Nucleic Acids Res* 35:7096–7108.

13. Miyagi E, et al. (2007) Enzymatically active APOBEC3G is required for efficient inhibition of human immunodeficiency virus type 1. *J Virol* 81:13346–13353.

14. Bishop KN, et al. (2008) APOBEC3G inhibits elongation of HIV-1 reverse transcripts. *PLoS Pathog* 4:e1000231.

15. Nathans R, et al. (2008) Small-molecule inhibition of HIV-1 Vif. *Nat Biotechnol* 26:1187–1192.

16. Hershko A, Ciechanover A (1998) The ubiquitin system. *Annu Rev Biochem* 67:425–479.

17. Pickart CM (2001) Mechanisms underlying ubiquitination. *Annu Rev Biochem* 70:503–533.

18. Skowyra D, et al. (1997) F-box proteins are receptors that recruit phosphorylated substrates to the SCF ubiquitin-ligase complex. *Cell* 91:209–219.

19. Mehle A, et al. (2004) Phosphorylation of a novel SOCS-box regulates assembly of the HIV-1 Vif-Cul5 complex that promotes APOBEC3G degradation. *Genes Dev* 18:2861–2866.

20. Stanley BJ, et al. (2008) Structural insight into the human immunodeficiency virus Vif SOCS box and its role in human E3 ubiquitin ligase assembly. *J Virol* 82:8656–8663.

21. Kobayashi M, et al. (2005) Ubiquitination of APOBEC3G by an HIV-1 Vif-Cullin5-Elongin B-Elongin C complex is essential for Vif function. *J Biol Chem* 280:18573–18578.

22. Mehle A, Thomas ER, Rajendran KS, Gabuzda D (2006) A zinc-binding region in Vif binds Cul5 and determines cullin selection. *J Biol Chem* 281:17259–17265.

23. Xiao Z, et al. (2006) Assembly of HIV-1 Vif-Cul5 E3 ubiquitin ligase through a novel zinc-binding domain-stabilized hydrophobic interface in Vif. *Virology* 349:290–299.

24. Pery E, Rajendran KS, Brazier AJ, Gabuzda D (2009) Regulation of APOBEC3 proteins by a novel YXXL motif in human immunodeficiency virus type 1 Vif and simian immunodeficiency virus SIVagm Vif. *J Virol* 83:2374–2381.

25. Russell RA, et al. (2009) Distinct domains within APOBEC3G and APOBEC3F interact with separate regions of human immunodeficiency virus type 1 Vif. *J Virol* 83:1992–2003.

26. Schröfelbauer B, Senger T, Manning G, Landau NR (2006) Mutational alteration of human immunodeficiency virus type 1 Vif allows for functional interaction with nonhuman primate APOBEC3G. *J Virol* 80:5984–5991.

27. Bogerd HP, Doehle BP, Wiegand HL, Cullen BR (2004) A single amino acid difference in the host APOBEC3G protein controls the primate species specificity of HIV type 1 virion infectivity factor. *Proc Natl Acad Sci USA* 101:3770–3774.

28. Mangeat B, Turelli P, Liao S, Trono D (2004) A single amino acid determinant governs the species-specific sensitivity of APOBEC3G to Vif action. *J Biol Chem* 279:14481–14483.

29. Schröfelbauer B, Chen D, Landau NR (2004) A single amino acid of APOBEC3G controls its species-specific interaction with virion infectivity factor (Vif). *Proc Natl Acad Sci USA* 101:3927–3932.

30. Xu H, et al. (2004) A single amino acid substitution in human APOBEC3G antiretroviral enzyme confers resistance to HIV-1 virion infectivity factor-induced depletion. *Proc Natl Acad Sci USA* 101:5652–5657.

31. Huthoff H, Malim MH (2007) Identification of amino acid residues in APOBEC3G required for regulation by human immunodeficiency virus type 1 Vif and Virion encapsidation. *J Virol* 81:3807–3815.

32. Holden LG, et al. (2008) Crystal structure of the anti-viral APOBEC3G catalytic domain and functional implications. *Nature* 456:121–124.

33. Prochnow C, et al. (2007) The APOBEC-2 crystal structure and functional implications for the deaminase AID. *Nature* 445:447–451.

34. Eswar N, et al. (2006) Comparative protein structure modeling using Modeller. *Curr Protoc Bioinformatics* Chapter 5:Unit 5 6.

35. Kao S, et al. (2003) The human immunodeficiency virus type 1 Vif protein reduces intracellular expression and inhibits packaging of APOBEC3G (CEM15), a cellular inhibitor of virus infectivity. *J Virol* 77:11398–11407.

36. Xu H, et al. (2007) Stoichiometry of the antiviral protein APOBEC3G in HIV-1 virions. *Virology* 360:247–256.

37. Chen KM, et al. (2008) Structure of the DNA deaminase domain of the HIV-1 restriction factor APOBEC3G. *Nature* 452:116–119.

38. Furukawa A, et al. (2009) Structure, interaction and real-time monitoring of the enzymatic reaction of wild-type APOBEC3G. *EMBO J* 28:440–451.

39. Harjes E, et al. (2009) An extended structure of the APOBEC3G catalytic domain suggests a unique holoenzyme model. *J Mol Biol* 389:819–832.

40. Huthoff H, et al. (2009) RNA-dependent oligomerization of APOBEC3G is required for restriction of HIV-1. *PLoS Pathog* 5:e1000330.

41. Zhang KL, et al. (2007) Model structure of human APOBEC3G. *PLoS ONE* 2:e378.

42. Dang Y, Siew LM, Zheng YH (2008) APOBEC3G is degraded by the proteasomal pathway in a Vif-dependent manner without being polyubiquitylated. *J Biol Chem* 283:13124–13131.

43. Gooch BD, Cullen BR (2008) Functional domain organization of human APOBEC3G. *Virology* 379:118–124.

44. Zheng N, et al. (2002) Structure of the Cul1-Rbx1-Skp1-F boxSkp2 SCF ubiquitin ligase complex. *Nature* 416:703–709.

45. Scherer DC, et al. (1995) Signal-induced degradation of I kappa B alpha requires site-specific ubiquitination. *Proc Natl Acad Sci USA* 92:11259–11263.

46. Stroschein SL, Bonni S, Wrana JL, Luo K (2001) Smad3 recruits the anaphase-promoting complex for ubiquitination and degradation of SnoN. *Genes Dev* 15:2822–2836.

47. Orlicky S, et al. (2003) Structural basis for phosphodependent substrate selection and orientation by the SCFCdc4 ubiquitin ligase. *Cell* 112:243–256.

48. Iwatani Y, Takeuchi H, Strebel K, Levin JG (2006) Biochemical activities of highly purified, catalytically active human APOBEC3G: Correlation with antiviral effect. *J Virol* 80:5992–6002.

Supporting Information

Iwatani et al. 10.1073/pnas.0906652106

SI Text

Plasmids and Antibodies. A3G expression plasmids were constructed using pcDNA-A3G that contains a C-terminal MycHIS tag (consisting of Myc and (His)$_6$ (HIS) epitopes) (1, 2). Arg substitutions for A3G Lys residues and the two Lys residues in the C-terminal tag (Lys-free MycHIS tag), as well as Gln substitution for Glu-259 at the A3G catalytic center were introduced into pcDNA-A3G by using the QuikChange XL Site Directed Mutagenesis Kit (Stratagene). For all mutants, the nucleotide sequences of both the insert and the boundary regions were verified by DNA sequencing. pcDNA-HVif, a human codon-optimized clone used for Vif expression (3), was a generous gift from Dr. Klaus Strebel (NIAID, NIH).

A3G's sensitivity toward HIV-2 and SIV$_{mac}$ Vif was tested using the appropriate expression plasmids: vif(+) plasmids, pGH-123 (4) and pMA239 (5), respectively; and vif(-) control plasmids, pGH-Xb (4) and pMA-Sc (5), respectively (generously provided by Dr. Akio Adachi, University of Tokushima). In connection with construction of a SupT1 cell line that stably expresses A3G (see below), A3G cDNA fragments were inserted into the plasmid, pRetroX-Tight-Pur (Clontech) using NotI and MluI restriction sites. The resulting plasmids that express A3G WT, S-A3G, and A3G D128K (without a tag), were designated as pRetroX A3G WT, pRetroX S-A3G, and pRetroX A3G D128K, respectively. To produce virus that can be pseudotyped with the Vesicular Stomatitis virus env gene (VSV-G), the clone pNLucvif(-) was constructed using the luciferase-expressing, HIV-1 env-negative pNL4-3 derivative, pNLuc (generous gift from Dr. Eric O. Freed, NIH, NCI-Frederick) (6), and pNL4-3vif(-).

A peptide antibody (C-17 rabbit serum) against human A3G, anti-Vif antibody, and anti-p24 (CA) rabbit serum were obtained from the AIDS Research and Reference Reagent Program, catalog no. 10082, 2221, and 4250, respectively. Anti-Myc tag mAb (9B11, Cell Signaling Technology), anti-HIS tag rabbit serum (Medical & Biological Laboratories Co.), and β-tubulin rabbit polyclonal antibody (Abcam) were purchased from the respective companies.

Preparation of SupT1 Cells Stably Expressing A3G. For efficient expression of A3G in T-cell lymphocytes, it was necessary to construct SupT1 cells that stably express A3G. These cells were generated using the retroviral gene transfer system "Retro-X Tet-Off Advanced inducible Expression System" (Clontech), following the manufacturer's protocol. Briefly, retroviral vectors were produced by cotransfection of 293T cells with pVSV-G (Clontech), the murine leukemia virus Gag/Pol expression plasmid pMLVg/p (7), and pRetroX-Tight-Pur vector-based A3G expression plasmids or the empty vector. In addition, a retroviral vector for expression of Tet-Off transactivator was prepared by cotransfection of 293T cells with pVSV-G, pMLVg/p, and pRetro-X-Tet-Off Advanced (Clontech). SupT1 cells were serially infected with the retroviral vector for the Tet-Off transactivator and subsequently, with the A3G vector. Cells that were resistant to both G418 (500 ng/mL) (Roche) and Puromycin (1

mg/mL) were selected and doubly transfected stable cell lines expressing no A3G, A3G WT, A3G D128K, and S-A3G were designated as SupTetOff, SupTetOff A3G WT, SupTetOff A3G D128K, and SupTetOff S-A3G, respectively.

Assay of Vif-Dependent Degradation of A3G. A3G or mutant A3G expression plasmids (2 μg) and pcDNA-HVif or pcDNA 3.1 (-) control (i.e., empty) vector (4 μg) were cotransfected into Human Embryonic Kidney cells (293T) in 6-well plates, using FuGENE HD (Roche). Forty-eight hours post transfection, cell lysates were prepared in Laemmli buffer (Bio-Rad) containing 2.5% 2-mercaptoethanol (ME). Cell lysates were subjected to SDS/PAGE and the proteins were transferred to Immobilon-P membranes (Millipore). The membranes were first incubated with appropriate antibodies, as specified, and were then incubated with horseradish peroxidase-conjugated secondary antibodies (Pierce). Proteins were visualized by enhanced chemiluminescence, using SuperSignal West Dura (Pierce).

For Vif-dependent degradation of A3G in T-lymphocytes, SupTetOff cells expressing A3G (1 × 10^5 cells) were infected with VSV-G pseudotyped viruses (200 ng); NL4-3 WT or NL4-3 vif(-) were produced by cotransfection of 293T cells with pVSV-G and either pNLuc or pNLuc vif(-). At 72 h post infection, cell lysates were prepared and A3G expression was evaluated by Western blot analysis.

Detection of Polyubiquitinated A3G. 293T cells were cotransfected with A3G expression plasmid (Lys-free MycHIS tag) and pcDNA-HVif, plus either myc-tagged ubiquitin (Ub) or the mutant K48R (Arg substitution at Ub residue Lys-48) (8). Forty-eight hours post transfection, cells were lysed with 6M urea in PBS, the expressed A3G was pulled-down using TALON resin (Clontech) and proteins were detected by Western blot analysis using anti-A3G antibody.

Infectivity Assays Using LuSIV Cells. Virus production and analysis of virus infectivity were performed as reported previously (1). Briefly, to obtain virus particles, 293T cells were cotransfected with 4 μg of pNL4-3 WT and/or pNL4-3vif(-) (ratios as described in the main text) plus 2 μg of pcDNA-A3G or pcDNA 3.1 (-) (vector control). Virus infectivity was determined by single-cycle replication assays with LuSIV cells (9), obtained from the AIDS Research and Reference Reagent Program, NIAID, NIH (cells originally from Drs. J. W. Roos and J. E. Clements). Infectivity was calculated by normalizing for the amount of input CA, determined as p24 antigen by ELISA (ZeptoMetrix).

Incorporation of A3G into Virions. Cell-free-filtered supernatants from transfected 293T cells were pelleted (75 min, 151,000 × g) through a 20% sucrose cushion in an SW41 rotor, as previously described (1). The concentrated virus pellet was lysed in 1X Laemmli buffer containing 2-ME. Proteins were separated by SDS/PAGE (10% polyacrylamide gel) and were detected by immunoblotting with the appropriate antibodies.

1. Iwatani Y, Takeuchi H, Strebel K, Levin JG (2006) Biochemical activities of highly purified, catalytically active human APOBEC3G: Correlation with antiviral effect. J Virol 80:5992–6002.
2. Kao S, et al. (2003) The human immunodeficiency virus type 1 Vif protein reduces intracellular expression and inhibits packaging of APOBEC3G (CEM15), a cellular inhibitor of virus infectivity. J Virol 77:11398–11407.
3. Nguyen KL, et al. (2004) Codon optimization of the HIV-1 vpu and vif genes stabilizes their mRNA and allows for highly efficient Rev-independent expression. Virology 319:163–175.
4. Shibata R, et al. (1990) Mutational analysis of the human immunodeficiency virus type 2 (HIV-2) genome in relation to HIV-1 and simian immunodeficiency virus SIV (AGM). J Virol 64:742–747.

5. Shibata R, et al. (1991) Generation of a chimeric human and simian immunodeficiency virus infectious to monkey peripheral blood mononuclear cells. *J Virol* 65:3514–3520.
6. Kiernan RE, Ono A, Englund G, Freed EO (1998) Role of matrix in an early postentry step in the human immunodeficiency virus type 1 life cycle. *J Virol* 72:4116–4126.
7. Abudu A, et al. (2006) Murine retrovirus escapes from murine APOBEC3 via two distinct novel mechanisms. *Curr Biol* 16:1565–1570.
8. Mehle A, et al. (2004) Vif overcomes the innate antiviral activity of APOBEC3G by promoting its degradation in the ubiquitin-proteasome pathway. *J Biol Chem* 279:7792–7798.
9. Roos JW, et al. (2000) LuSIV cells: A reporter cell line for the detection and quantitation of a single cycle of HIV and SIV replication. *Virology* 273:307–315.

```
                  ΩΩΩΩΩ                                    ━━━━━▶                        ━━▶            ΩΩΩΩΩΩΩ
        10        20          30          40          50          60          70          80
MKPHFRNTVERMYRDTFSYNFYNRPILSRRNTVWLCYEVKTKGPSRPPLDAKIFRGQVYSELKYHPEMRFFHWFSKWRKL

           ━━━━━▶          ΩΩΩΩΩΩΩΩΩΩΩ       ━━━━━▶          ΩΩΩΩΩΩΩΩΩΩΩΩΩ          ━▶   ΩΩΩΩΩΩΩ
        90         100         110         120         130         140         150         160
HRDQEYEVTWYISWSPCTKCTRDMATFLAEDPKVTLTIFVARLYYFWDPDYQEALRSLCQKRDGPRATMKIMNYDEFQHC

ΩΩΩΩΩΩ               ΩΩΩΩΩΩΩΩΩΩΩΩΩ              ΩΩΩΩΩΩ       ━━▶    ━━━━━▶     ━━━
        170         180         190         200         210         220         230         240
WSKFVYSQRELFEPWNNLPKYYILLHIMLGEILRHSMDPPTFTFNFNNEPWVRGRHETYLCYEVERMHNDTWVLLNQRRG

      ━━━▶         ΩΩΩΩΩΩΩΩ           ━━━━━━▶      ΩΩΩΩΩΩΩΩΩΩΩΩΩ      ━━━━━▶
        250         260         270         280         290         300         310         320
FLCNQAPHKHGFLEGRHAELCFLDVIPFWKLDLDQDYRVTCFTSWSPCFSCAQEMAKFISKNKHVSLCIFTARIYDDQGR

   ΩΩΩΩΩΩΩ       ━━━━━▶    ΩΩΩΩΩΩΩΩΩΩΩ              ΩΩΩΩΩΩΩΩΩΩΩΩΩΩΩΩΩΩΩΩ
        330         340         350         360         370         380
CQEGLRTLAEAGAKISIMTYSEFKHCWDTFVDHQGCPFQPWDGLDEHSQDLSGRLRAILQNQEN
```

Fig. S1. Amino acid sequence of A3G. All 20 Lys residues are shown in blue, with the 14 most exposed amino acids in dark blue. The zinc-coordinating residues are colored orange. Every tenth amino acid is numbered and secondary structure elements are depicted above the sequence, with α-helices as coils and β-strands as arrows.
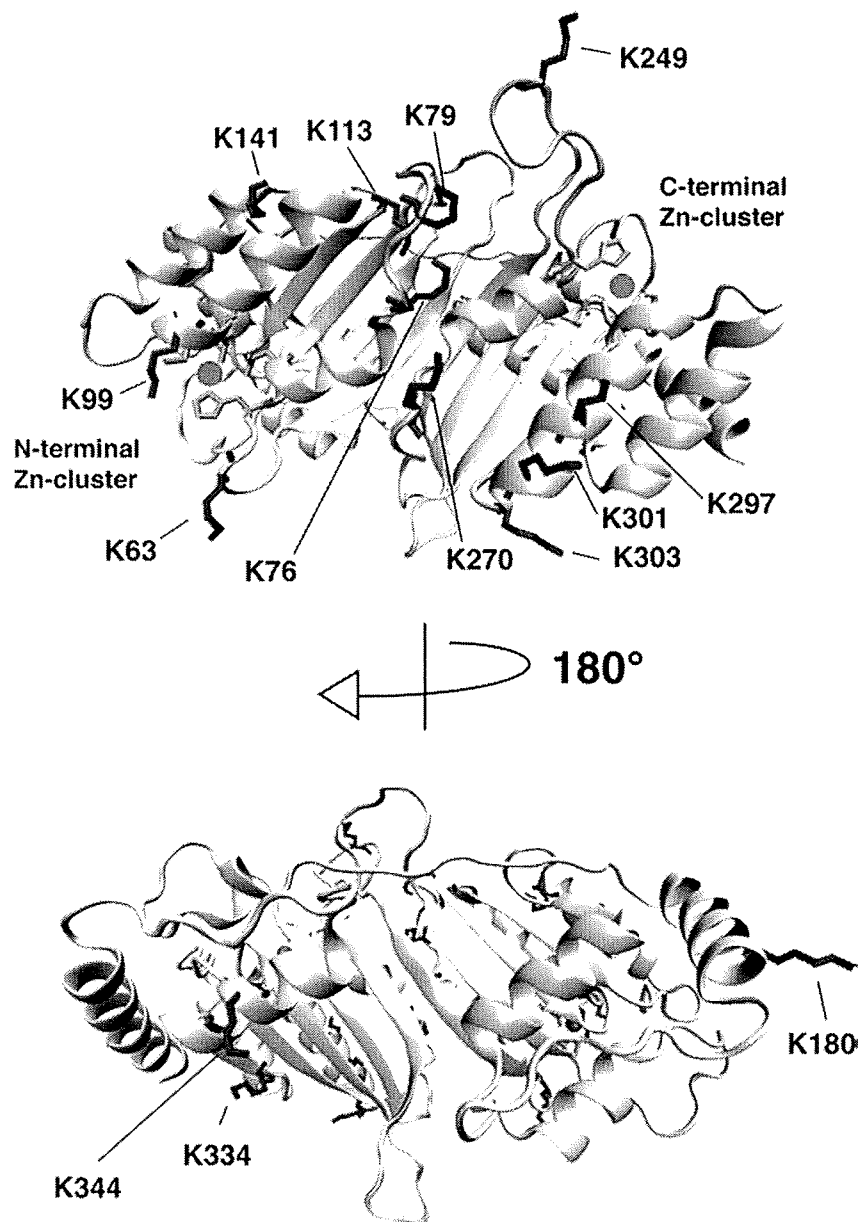
Fig. S2. Model structure of A3G. Ribbon diagram of full-length A3G in two different orientations with the side chains of the 14 most surface-exposed Lys depicted in stick representation (blue). The side chains of the Zn-coordinating residues in the NTD and CTD are also displayed and colored in orange and yellow, respectively. Positions of the zinc atoms are labeled by red spheres.
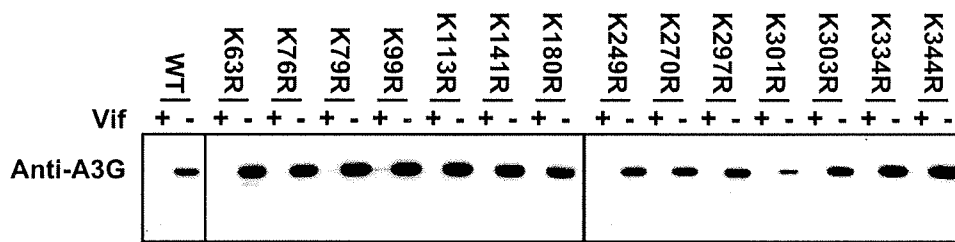
Fig. S3. Effect of single point mutations changing each of the 14 Lys residues to Arg on HIV-1 Vif sensitivity. Fourteen point mutants (K63R, K76R, K79R, K99R, K113R, K141R, K180R, K249R, K270R, K297R, K301R, K303R, K334R, and K344R) were constructed and assayed for A3G expression in the presence (+) or absence (−) of Vif, as described in the *SI Text*.
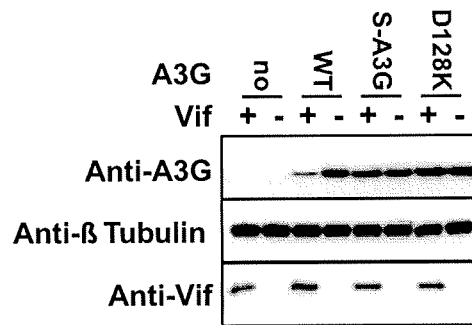
Fig. S4. Resistance of S-A3G to Vif-mediated degradation in SupT1 cells. SupT1 cells that stably express no A3G, A3G WT, S-A3G, or A3G D128K (SupTetOff, SupTetOff A3G WT, SupTetOff S-A3G, or SupTetOff A3G D128K, respectively) were prepared and infected with either VSV-G pseudotyped HIV-1 (+) or *vif*-deficient HIV-1 (−) viruses, as described in the *SI Text*. Protein expression in the absence or presence of Vif was assayed by Western blot analysis.
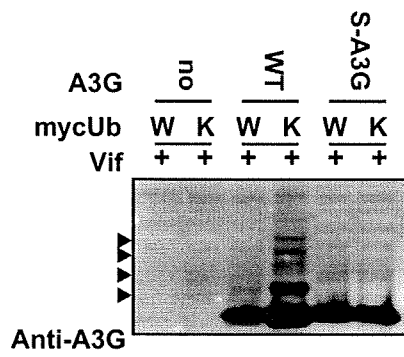
Fig. S5. Polyubiquitination of A3G mutants. 293T cells were cotransfected with Vif and the indicated A3G expression plasmids (Lys-free MycHIS tagged versions) plus either myc-tagged Ub (W) or the mutant K48R (K) expression plasmids. Ubiquitinated A3G proteins were pulled-down with TALON beads and detected by Western blot analysis using anti-A3G antibody. The positions of ubiquitinated A3G are indicated by the arrow heads.
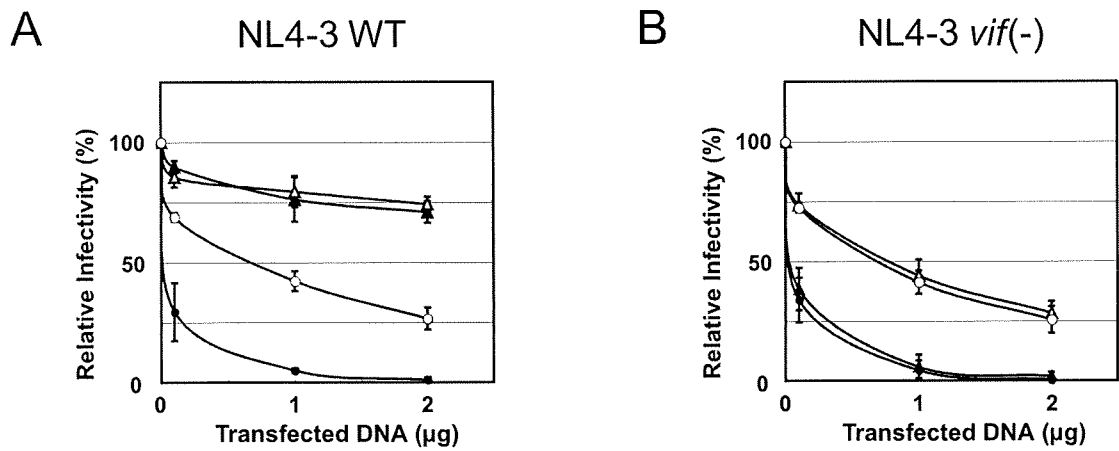
Fig. S6. Antiviral activity of A3G and S-A3G active-site mutants. 293T cells were cotransfected with (*A*) pNL4-3 and either A3G WT (▲), A3G E259Q (△), S-A3G (●), S-A3G E259Q (○) expression plasmids or (*B*) pNL4–3*vif*(-) and the indicated A3G expression plasmids, using 0.1, 1, or 2 μg of DNA. Amounts of added DNA for each of the expression plasmids were adjusted with empty vector pcDNA 3.1 (-) to a total of 2 μg. Infectivity is expressed relative to the values for 0 μg of the expression plasmids, set at 100%.

		297				301		303					334		
Homo sapiens	295 M A	K	F I S	K	N	K	H	- -	::	- G A	K	I S	336
Pan troglodytes	295 M A	K	F I S	N	N	K	H	- -	::	- G A	K	I S	336
Pan paniscus	295 M A	K	F I S	N	N	K	H	- -	::	- G A	E	I S	336
Pan pygmaeus	295 M A	K	F I S	N	N	Q	H	- -	::	- E A	K	I S	336
Gorilla gorilla	295 M A	K	F I S	N	K	K	H	- -	::	- G A	K	I S	336
Hylobates lar	230 M A	K	F I S	N	N	K	R	- -	::	- R A	K	I S	271
Nomascus leucogenys	288 M A	K	F I S	N	N	K	R	- -	::	- R A	K	I S	329
Macaca fascicularis	295 M A	K	F I S	N	N	E	H	- -	::	- G A	K	I A	336
Macaca nemestrina	287 M A	K	F I S	N	N	E	H	- -	::	- G A	K	I A	328
Macaca nigra	294 M A	K	F I S	N	N	E	H	- -	::	- G A	K	I A	335
Macaca mulatta	473 M A	K	F I S	N	N	E	H	- -	::	- G A	K	I A	328
Erythrocebus patas	294 M A	K	F I S	K	K	K	H	- -	::	- G A	K	I A	335
Papio anubis	294 M A	K	F I S	N	N	E	H	- -	::	- G A	K	I A	335
Cercopithecus aethiops	294 M A	K	F I S	N	N	K	H	- -	::	- G A	K	I A	335
Symphalangus syndactylus	283 M A	K	F I S	N	N	K	R	- -	::	- R A	K	I S	324

Fig. S7. Amino acid sequence comparison around the four C-terminal Lys residues of primate A3G proteins. Sequences were aligned by using MacVector 7.0 (MacVector, Inc.) software and residues at positions 297, 301 303, and 334 are enclosed in blue boxes. Lys residues at these positions are shown in red. The genbank accession numbers are: *Homo sapiens* (NP_068594); *Pan troglodytes* (AAT44392); *Pan paniscus* (AAT72156); *Pan pygmaeus* (AAT44395); *Gorilla gorilla* (AAT44394); *Hylobates lar* (ABB77894); *Nomascus leucogenys* (ABB77892); *Macaca fascicularis* (AAT44393); *Macaca nemestrina* (AAY99624); *Macaca nigra* (AAT44391); *Macaca mulatta* (AAP85256); *Erythrocebus patas* (AAT44390); *Papio anubis* (AAT44398); *Cercopithecus aethiops* (AAP85254); and *Symphalangus syndactylus* (ABB77893).
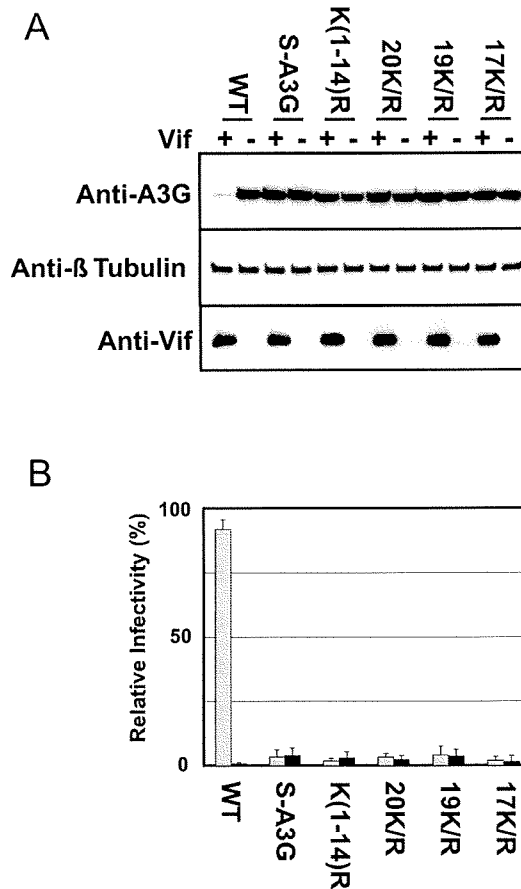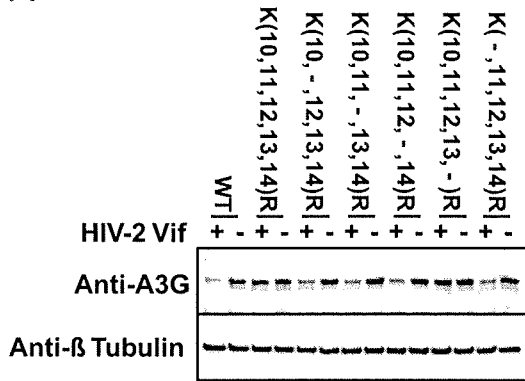
Fig. S8. Vif-dependent degradation (*A*) and antiviral activity (*B*) for various Lys to Arg substitution mutants of A3G. Designations for the different mutants are as follows: K(1–14)R at 63, 76, 79, 99, 113, 141, 180, 249, 270, 297, 301, 303, 334, and 344; 20K/R at 2, 40, 42, 52, 63, 76, 79, 99, 113, 141, 150, 163, 180, 249, 270, 297, 301, 303, 334, and 344; 19K/R at 40, 42, 52, 63, 76, 79, 99, 113, 141, 150, 163, 180, 249, 270, 297, 301, 303, 334, and 344; 17K/R at 40, 42, 52, 63, 76, 79, 99, 113, 141, 180, 249, 270, 297, 301, 303, 334, and 344. (*B*) 293T cells were cotransfected with 4 μg of either pNL4–3 (gray bar) or pNL4–3*vif*(-) (black bar), and 1 μg of the indicated A3G expression plasmid. Virus infectivity was measured using LuSIV cells, as described in the *SI Text*. Infectivity values are given relative to the value for the vector control, which was set at 100%.
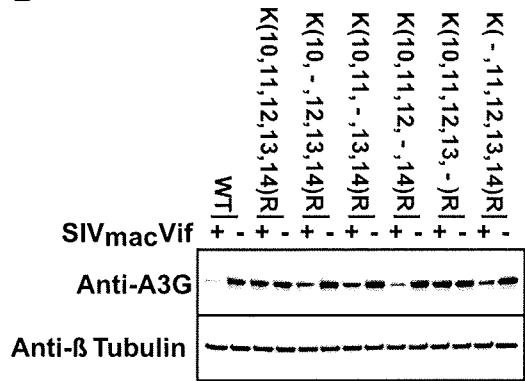
A

	WT	K(10,11,12,13,14)R	K(10, - ,12,13,14)R	K(10,11, - ,13,14)R	K(10,11,12, - ,14)R	K(10,11,12,13, -)R	K(- ,11,12,13,14)R
HIV-2 Vif	+ -	+ -	+ -	+ -	+ -	+ -	+ -

Anti-A3G

Anti-ß Tubulin

B

	WT	K(10,11,12,13,14)R	K(10, - ,12,13,14)R	K(10,11, - ,13,14)R	K(10,11,12, - ,14)R	K(10,11,12,13, -)R	K(- ,11,12,13,14)R
SIVmacVif	+ -	+ -	+ -	+ -	+ -	+ -	+ -

Anti-A3G

Anti-ß Tubulin

Fig. S9. A3G mutant sensitivity toward HIV-2 and SIV$_{mac}$ Vif proteins. Assays for Vif-dependent degradation were performed using HIV-2 and SIV$_{mac}$ Vif expression plasmids, pGH123 and pMA239, respectively. For the corresponding Vif-negative controls, pGH-Xb and pMA-Sc were used, respectively.

第 9 回 ECC 山口メモリアルエイズ研究奨励賞受賞研究

宿主防御因子 APOBEC3G の抗 HIV 作用メカニズムに関する研究
Study on Molecular Mechanism of Host Defense Factor,
APOBEC3G, against HIV

岩 谷 靖 雅

Yasumasa IWATANI

（独）国立病院機構　名古屋医療センター臨床研究センター　感染・免疫研究部

Department of Microbiology and Immunology, Clinical Research Center,
National Hospital Organization Nagoya Medical Center

はじめに

今回, 第 9 回日本エイズ学会 ECC 山口メモリアルエイズ研究奨励賞受賞の背景となった研究について, 概説する。

研究の背景

宿主防御因子 APOBEC3G （A3G） は細胞内に発現する Cytidine Deaminase （ssDNA 中の Cytidine を脱アミノ化し, dU に変換する酵素）で, レトロウイルスに対する宿主防御因子である。A3G は, Vif を欠損した HIV-1 （以下, HIV-1*vif* （-）） の複製を強く阻害する。HIV-1*vif* （-） は, ウイルス産生細胞内で発現する A3G を粒子内に取込む。そのため, 新たな細胞に感染する時に, 逆転写の過程が A3G によって強く阻害される。一方, 野生型の HIV-1 （以下, HIV-1 WT） は, ウイルス産生細胞内で Vif を発現し, ユビキチン/プロテアソーム系を介して選択的に A3G を破壊し枯渇させてしまう。このため, HIV-1 WT は A3G をウイルス粒子に取込まず, A3G の防御システムから逃れることができる （図 1）。A3G の抗レトロウイルス作用の分子メカニズムについては, 諸説あるが, Cytidine Deaminase としての酵素活性に依存的な機構と非依存的なメカニズムがあることまでは一致した見解である。その根拠は 2 つある。1) 酵素活性を欠失した A3G は, 野生型より低いが, 発現量依存的に抗 HIV 作用を示す。特に, 過剰発現させた場合には, 野生型の効果に匹敵する。2) A3G は, B 型肝炎ウイルスやパルボウイルス, いくつかのレトロトランスポゾンに対しても強い抗ウイルス作用 （DNA 合成阻害） を示すが, いずれも Deaminase 非依存的に抑制する。

著者連絡先：〒460-0001　名古屋市中区三の丸 4-1-1　独立行政法人国立病院機構　名古屋市医療センター臨床研究センター

実は, 「細胞が HIV-1*vif* （-） の増殖を許容するか否かを決定する因子が A3G である」 という発見以前から, 非許容細胞 （A3G を発現する細胞） から産生される HIV-1*vif* （-） の感染では, 感染細胞内における逆転写反応が抑制され, 逆転写初期から後期にかけて逆転写産物が段階的に減少することが分かっていた。さらに, この抑制効果はターゲット細胞がどんな細胞種であれ同様に認められることが分かっていた。A3G が広範な抗ウイルス作用スペクトルを示すことを考慮すると, A3G の抗 HIV 作用機序は, A3G がもつ何らかの分子生化学的特性が, 細胞質で DNA 合成をするウイルス （HBV やパルボウイルス, いくつかのレトロエレメント） に共通した分子機序に帰結することがもっともらしいと考えられる。

多くの研究者が感染細胞を用いた研究により, 抗 HIV 作用機構の解明に取り組んでいる。しかし, 図 2 に示したような HIV の複雑な逆転写過程について各ステップを, 感染細胞を用いて評価することは非常に困難である。そのため, 逆転写がどのように抑制されるのかという分子レベルでの詳細な機序は明らかになっていなかった。そこで, 筆者は A3G タンパクを精製し, A3G の生化学的, 分子生物学的な性質を明らかにし[1], *in vitro* 再構築系を用いて逆転写の各過程に対する影響を解析し, 抗 HIV 作用機序を分子レベルで明らかにする研究を行った。その結果, A3G の抗 HIV 作用メカニズムの 1 つである酵素活性非依存的な分子機序を明らかにすることができた[2]。以下, その結果について概説する。

A3G による酵素活性非依存的な HIV-1 逆転写阻害メカニズム

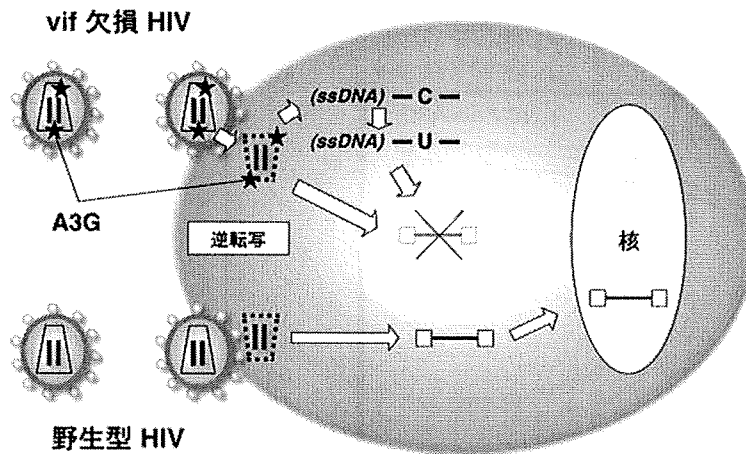最初に, 酵素活性をもつ A3G を, バキュロウイルスを用いた発現系を利用して発現・精製した[1]。筆者らが開発した *in vitro* の逆転写再構築系[3]を用いて, HIV-1 の一連の

図 1 A3G による抗 HIV 作用
vif を欠損した HIV では，ウイルス産生細胞由来の A3G がウイルス粒子（コア）に取込まれ，新たに感染した細胞において逆転写産物が減少する。A3G による Cytidine Deaminase（酵素）活性依存的あるいは非依存的に阻害されるメカニズムがある。一方，野生型 HIV では，産生細胞内で Vif により A3G が枯渇させられるため，ウイルスは A3G を取込まず，A3G の抗ウイルス防御システムから逃れることができる。
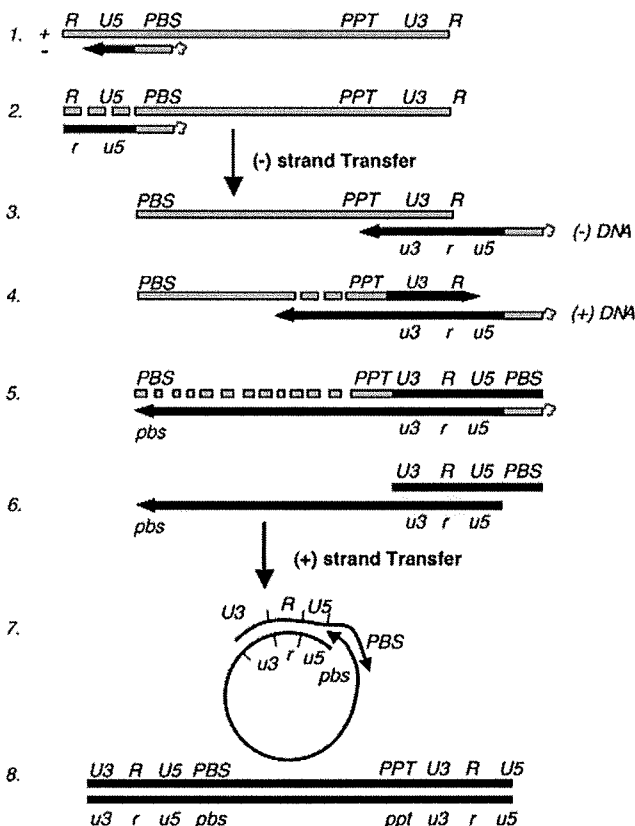

図 2 HIV の一連の逆転写複製過程
1；RT により，ゲノム RNA にアニーリングした tRNA から DNA 合成がスタートする（（−）SSDNA 合成）。2；RNaseH により，（−）SSDNA の鋳型 RNA が消化される（RNaseH Cleavage）。3；NC の Chaperone 活性により（−）SSDNA が下流の再アニーリングする（（−）Strand Transfer）。4；RNaseH による PPT 領域 RNA 以外の消化と，PPT をプライマーとした DNA 伸長反応がはじまる（PPT Processing と PPT Initiation）。5；（−）と（＋）鎖合成ともに PBS 末端まで到達し，鋳型 RNA は消化される。さらに，tRNA が RNaseH により取り除かれ PBS 領域の DNA が一本鎖となる（tRNA removal）。6 & 7；PBS 領域がアニーリングし（（＋）Strand Transfer），DNA 伸長反応が両方向に進む。8；RT の伸長反応が進み，完全長の 2 本鎖 DNA（プロウイルス DNA）がつくられる。

逆転写反応（図 2）において，A3G がどの過程に影響を与えるのか解析した。
　まず，逆転写のプライマーである tRNA$_3^{lys}$ と鋳型 RNA とのアニーリング反応に対する影響を検討した。ウイルス粒子内では，このアニーリングはウイルスタンパク NC（Nucleocapsid）の chaperone 機能によって行われる。図 3A
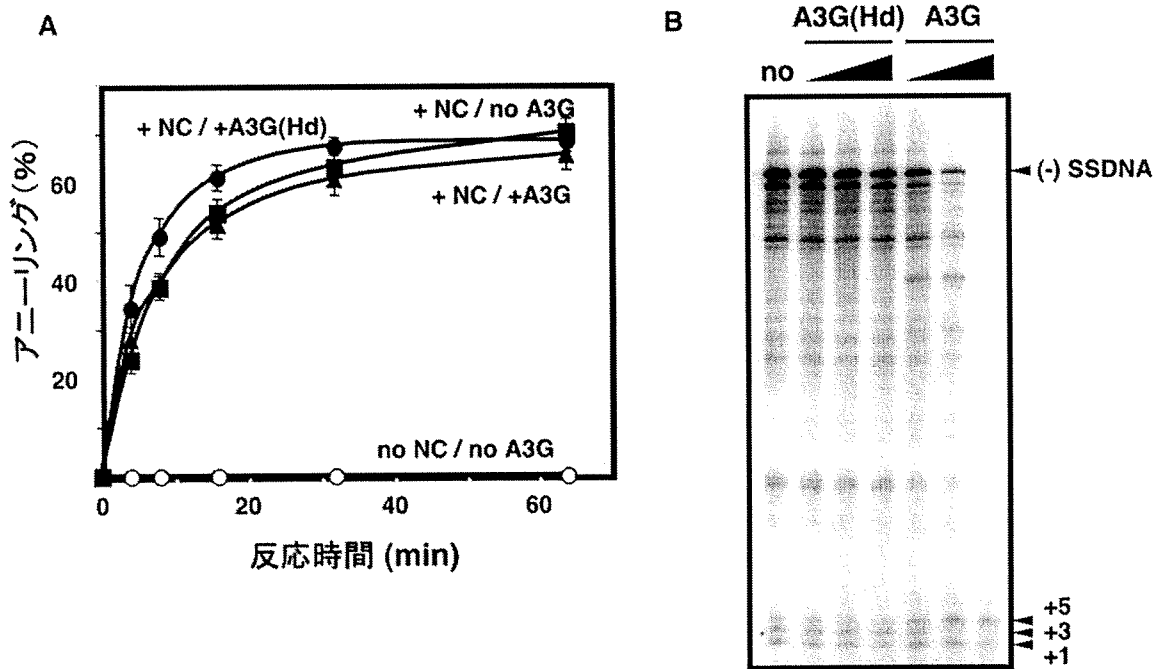
A

B

図 3 *in vitro* における A3G による tRNA アニーリングおよび tRNA からの （−） SSDNA 合成開始反応に対する影響
A ; NC による tRNA アニーリング反応速度に対する A3G の影響を解析した。NC （核酸 7 base あたり 1 分子）
量を，A3G （80 nM） を加えた。B ; 熱変性させた A3G と未変性 A3G を加え，（−） SSDNA 合成を比較した。
1 （0 nM），2 & 5 （20 nM），3 & 6 （40 nM），4 & 7 （80 nM）。

に示したように，NC 非存在下 (noNC/noA3G) では，60 分
後でもアニーリングしない。NC 添加によってアニーリン
グが促進されるが （+NC/noA3G），そこに A3G （+NC/
+A3G） あるいは熱変性した A3G （+NC/+A3G （Hd））
を加えても，アニーリング速度は変化しなかった。つまり，
A3G は tRNA の Primer Placement の過程には影響を与え
ないことが示された。それに反して，tRNA^{lys}からはじま
る逆転写伸長反応 （（−） SSDNA 合成）（（−） SSDNA :
minus-strong stop DNA）は，A3G の濃度依存的に強く抑制
された （図 3B）。ちなみに，A3G を添加しない場合あるい
は熱変性した A3G では，その抑制効果は認められなかっ
た。さらに，（−） SSDNA 合成速度を調べた結果，RNA 鋳
型 1 分子あたり 13 分子の A3G 存在比の場合では，約 1/24
に低下した。さらに，興味深いことに，A3G により，（−）
SSDNA 合成の Pausing Products （停止した中間産物） が多
く認められた。それらの Pausing Products を解析し鋳型
RNA の二次構造と照らし合わせた結果，A3G による （−）
SSDNA 伸長停止が鋳型 RNA 二次構造上のループやバル
ジで起こっていることが分かった。このことは，一本鎖核
酸 (ssDNA と ssRNA) に特異的に結合する A3G が，RNA
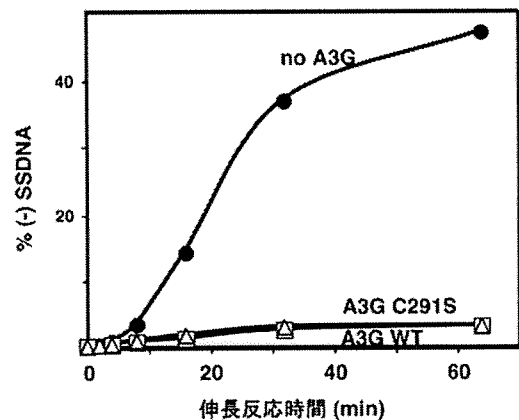の一本鎖領域に結合することによるものであると考えられ
た。

図 4 （−） SSDNA 合成阻害効果に対する A3G 酵素活
性の影響
野生型 A3G （0 nM） （●），野生型 A3G （80 nM）
（□），酵素活性欠損型 A3G C291S （80 nM） （△）
存在下で，（−） SSDNA 合成量を経時的に測定
した。

次に，A3G による （−） SSDNA 合成阻害が A3G の酵素
活性に依存するのか調べてみた。酵素活性中心に変異を導
入した A3G C291S タンパクを発現・精製し，（−） SSDNA

合成に対する抑制効果を解析した（図4）。その結果，A3G C291S も野生型と同等の抑制効果があることが分かった。これらの結果から，A3G の（−）SSDNA 合成抑制効果は，酵素活性非依存的におこることが明らかになった。さらに，RNaseH の切断反応に対する A3G の影響を調べた。その結果，RNaseH の切断速度かつ切断パターンは，A3G 添加によって影響を受けなかった。

（−）および（＋）Strand Transfer 反応においても，NC による Transfer アニーリング反応および伸長反応を含む全反応（Transfer 反応）に対する A3G の影響を解析した。これらの結果，A3G は，NC が介在するアニーリング反応自身には影響を与えずに，逆転写酵素（RT）が関わる伸長反応を含んだ Transfer 反応を阻害した。以上のことから，A3G は一連の逆転写の過程で，RT が関与するすべての伸長反応だけに抑制的に働くことが分かった。プルダウン法などによって A3G と RT の安定した直接的な結合は認められないことから，鋳型の核酸を介していると考えられた。

では，なぜ A3G は RT 伸長反応を阻害するが，同じく核酸結合タンパクである NC は抑制効果を示さないのか？この問いに答えるために，A3G と NC の核酸への結合特性の違いについて比較してみた。まず，蛍光ラベルした ssDNA（20 mer）を用いた蛍光偏光解消法により，HIV-1 NC と RT, A3G の解離定数（Kd）を測定した。その結果から，A3G（Kd : 238 nM）と NC（84.1 nM）は，RT（Kd : 1840 nM）を核酸から効率よく競合的に除外することがで

きるが，A3G は NC を核酸から容易には排除できない可能性が示唆された。さらに，一分子 DNA の光学機械的な伸展測定（Single Molecule DNA Stretching 解析）を行い，NC と A3G の核酸への結合解離（On/Off Rate）状態および核酸のアニーリングへの影響を検討した（図5）。NC は S 曲線が低く，R 曲線との違いが少ない。つまり，二本鎖 DNA を簡単に解す反面，アニーリングの際（R 曲線）NC は早く一本鎖領域から解離する。一方，A3G では S と R 曲線の違いが大きく，A3G は一本鎖領域に長時間結合し続け解離しないことが示された。以上のことから，A3G は NC に比べ，核酸への On/Off Rate が非常に遅いことが明らかになった。

これらの一連の研究から，A3G による酵素活性非依存的な抗 HIV 作用メカニズムは，A3G が鋳型である核酸の一本鎖領域に結合し，物理的に RT の伸長反応を阻害してしまうことによると考えられた（図6）。この阻害メカニズムは，RT と NC, A3G の核酸への結合特性によって決定されることが示された。

おわりに

本研究では，A3G の酵素活性非依存的な分子メカニズムについて明らかにした。最近，筆者が提唱した分子モデルを支持する in vivo の報告がなされている[4,5]。しかし，酵素活性依存的な機序に関しては依然として不明である。筆者が用いた in vitro 再構築系では足りない他の因子が関与している可能性がある。細胞内には，本来 DNA 中に存
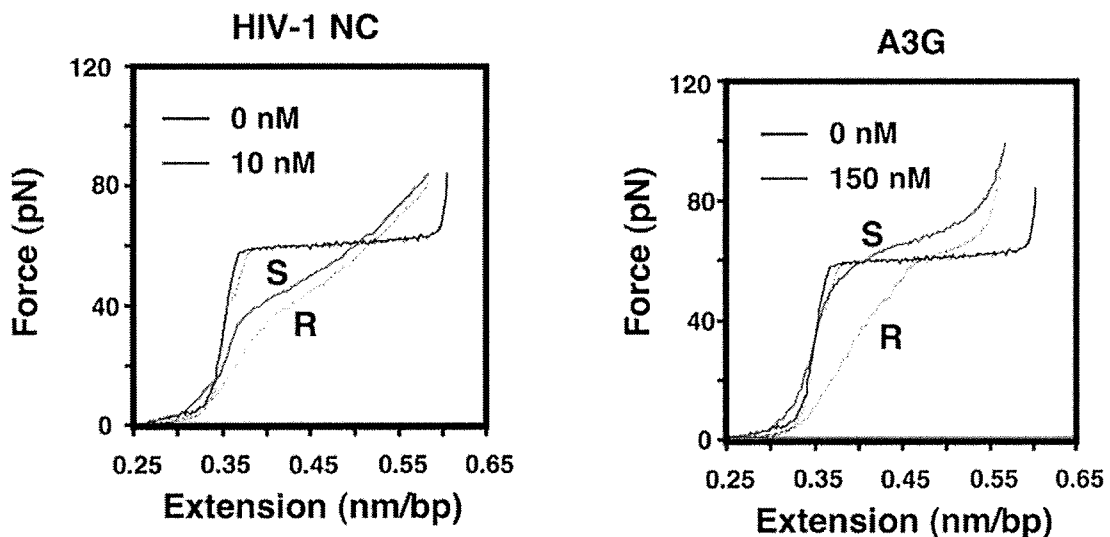
HIV-1 NC
A3G

図 5 1分子 DNA ストレッチング法を用いた A3G の核酸結合特性の解析
λDNA（二本鎖）1分子を光学機械的に伸展させ，HIV-1NC（10 nM）あるいは A3G（150 nM）存在下（赤）で，伸長（Extension）対付加（Force）を計測した。伸展（S : Streched）を実線，回復（R : Relaxed）を点線で示す。